energies

MDPI

Article

Development of Solid-State Lithium-Ion Batteries (LIBs) to Increase Ionic Conductivity through Interactions between Solid Electrolytes and Anode and Cathode Electrodes

Majid Monajjemi [1,*] and Fatemeh Mollaamin [2]

[1] Department of Chemical Engineering, Central Tehran Branch, Islamic Azad University, Tehran P.O. Box 1496969191, Iran
[2] Department of Biomedical Engineering, Faculty of Engineering and Architecture, Kastamonu University, Kastamonu 37150, Turkey; fmollaamin@kastamonu.edu.tr
* Correspondence: maj.monajjemi@iauctb.ac.ir

Abstract: Although in general ions are not able to migrate in the solid-state position due to rigid skeletal structure, in some solid electrolytes with a low energy barrier and high ionic conductivities, these ion transition can occur. In this work, we considered several solid electrolytes including lithium phosphorus oxy-nitride (LIPON), a lithium super-ionic conductor (SILICON), and thio-LISICON. For the fabrication and characterization of the solid electrolyte's fabrication, we used a single-step ball milling (SSBM) procedure. Through this research on all-solid-state rechargeable lithium-ion batteries, our target is to discuss solving several problems in solid LIBs that have recently escalated due to raised concerns relating to safety hazards such as solvent leakage and the flammability of the liquid electrolytes used for commercial LIBs. Through this research, we tested the conductivity amounts of various substrates containing amorphous glass, SSBM, and glass-ceramic samples. Obviously, the SSBM glass-ceramics increased the conductivity, and we also found that the values for conductivity attained by SSBM were higher than those values for glass-ceramics. Using an SSBM technique, silicon nanoparticles were used as an anode material and it was found that the charge and discharge curves in the battery cell cycled between 0.009 and 1.45 V versus Li^+/Li at a current density of 210 mA g^{-1} at room temperature. Since high resistance causes degradation between the cathode material ($LiCoO_2$) and the solid electrolyte, we added GeS2 and SiS_2 to the Li_2S-P_2S_5 system to obtain higher conductivities and better stability of the electrode–electrolyte interface.

Keywords: solid electrolytes; lithium-ion batteries; ionic conductivity; cathode materials; lithium phosphorus oxy-nitride (LIPON); single step ball milling (SSBM); lithium super-ionic conductor (SILICON)

Citation: Monajjemi, M.; Mollaamin, F. Development of Solid-State Lithium-Ion Batteries (LIBs) to Increase Ionic Conductivity through Interactions between Solid Electrolytes and Anode and Cathode Electrodes. *Energies* **2024**, *17*, 4530. https://doi.org/10.3390/en17184530

Received: 7 July 2024
Revised: 27 July 2024
Accepted: 28 July 2024
Published: 10 September 2024

1. Introduction

Although with advanced technologies liquid electrolytes are the most frequently used electrolyte application for LIB fabrication, the use of these types of electrolytes is hazardous and flammable in batteries. Therefore, in order to fabricate LIBs with an extreme degree of safety, liquid electrolytes should be exchanged for solid electrolytes. Solid electrolytes have several advantages compared to liquid electrolytes, including high stability, long life and durability, being non-flammable, and insulation to prevent thermal increase inside internal circuits. Moreover, these batteries do not need extra safety layers, which can cause the overall energy density to remain at high voltages and amperages [1–5]. In addition, based on particular phenomena in solid electrolytes (such as the fact that only Li^+ ions are mobile in solid electrolytes), several unfavorable parallel chemical reactions can be removed from the electrolytes, which causes the safety condition to be increased [6–9]. It is notable that, besides these advantages, there are some disadvantages; for instance, solid-state electrolytes (SSE) are not comparable with liquid electrolytes due to a lower achievable

conductivity. Our target in this study is a discussion on functional solid electrolyte LIBs to understand the action of the electrochemistry phenomenon. This work consists of a developmental concept of solid electrolytes for manufacturing methods and a characterization of these types of electrodes. The initial step in this research was accomplished to synthesize and characterize suitable conducting solid electrolytes. Interpreting the electrochemical properties for quick ion conduction via solid compounds is the key to the fabrication of solid-electrolyte LIBs [10–15]. A proper understanding of chemical reactions inside the LIBs can be yielded through using cathode mixed materials, as well as from the selection of proper composites for anodes during electrolyte–electrode interaction. Finally, our third target was to find the condition of a high-energy-density solid electrolyte rechargeable battery due to the efficiency of the kinetic reactions of cathode and anode compounds resulting from a decrease in nanoparticle sizes through electrochemical testing [15–20]. Through this research on all-solid-state rechargeable lithium-ion batteries, our target is to discuss solutions to several problems in solid LIBs that have recently escalated due to raised concerns relating to safety hazards such as solvent leakage and the flammability of the liquid electrolytes used for commercial LIBs. Since solid-state electrolytes do not inherently carry the safety burdens of liquid electrolytes, a large worldwide attempt is underway to provide a viable solid electrolyte instead of liquid electrolytes. Beyond the obvious safety advantages of solid electrolytes, all-solid-state batteries can be constructed with a wide variety of solid electrolyte products, varying in form and design and having high reliability.

2. Theoretical Backgrounds

Rechargeable LIBs work by charging and discharging, alternatively, through the exchange of Li^+ inside electrolytes via cathode and anode electrodes. The lithium diffusion process begins due to a current of Li^+ via the electrolyte, through a redox reaction and also through an external circuit (Scheme 1).

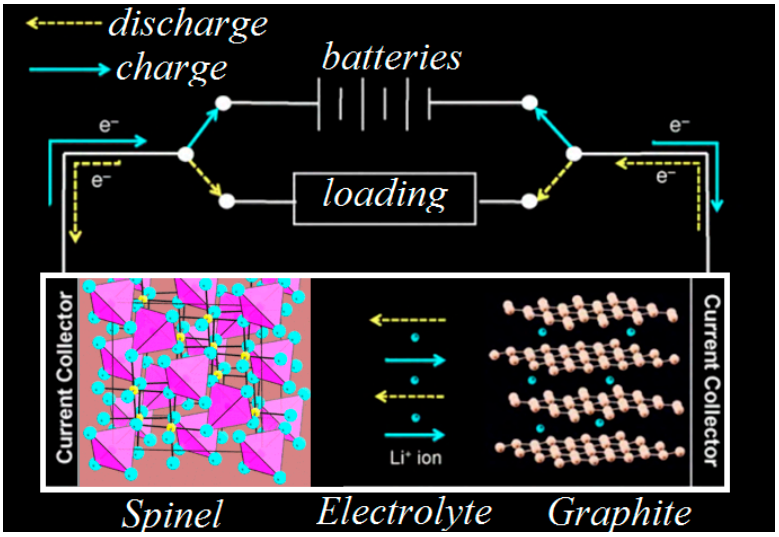

Scheme 1. Operating LIBs.

2.1. Ionic Position in Cathode Materials

The insertion of Li^+ inside cathode materials is largely related to the potential interaction among all ions, particularly the Li^+ and the host compounds. Obviously, the insertion of Li^+ in a crystal should be calculated, and it is ascertained that ion transport was accomplished through an optimal potential. Based on the shape of the insertion in the crystal, several structure items can be presented and be categorized, for example, $LiFePO_4$, similar structures to $LiCoO_2$, and 3D arrays of $LiMn_2O_4$ tunnels. The cathode materials directly affect insertion amounts of the Li ion as can be seen in Table 1. $LiCoO_2$

with two-dimensional layered structures was found to have the largest Li ion diffusivity amongst the classes, while $LiFePO_4$ with one-dimensional channels was found to have the lowest. Recently, several quantum chemical calculations of $LixCoO_2$ diffusivity have been accomplished at various amounts of Li ($0 \leq x \leq 1$), which indicate the reason for the width of the range of lithium's presence in electrolytes (Tables 1 and 2).

Table 1. Resistivity of cathode and anode electrodes.

Electrode	Compound	Band Gap (eV)	Conductivity Scm^{-1}	Reference
anode	Copper	0	6×10^5	[21,22]
anode	Graphite	0	2×10^3	[23,24]
anode	Aluminum	0	3.5×10^5	[25]
cathode	$LiCoO_2$	0.6–2.5	10^{-5}	[26–28]
cathode	$LiMn_2O_4$	0.25–2.1	10^{-4}	[29–31]
cathode	$LiFePO_4$	0.2–0.9	10^{-6}	[32,33]

Table 2. Ionic conductivities of various solid-state electrolytes (SSEs).

Cathode Composite	Electrical Conductivity (Scm^{-1})	Technique	Reference
Li_xCoO_2	2.1×10^{-2}	4 Point Probe DC	[34]
$Li_{1.0}Mgy\ Co_{1-y}O_2$	($10^{-3.77}$: y = 0); ($10^{-1.2}$: y = 0.04); ($10^{-0.70}$: y = 0.05)	4 Point Probe DC	[35]
$Li_xNi_{0.30}Co_{0.70}O_2$	10^{-4} to 10^{-3}: $0.70 < x < 1$	4 Point Probe DC	[36]
$LiGa_y\ Co_{1-y}O_2$	6.65×10^{-4}: un-doped system	EIS	[37]
$Li_xMn_2O_4$	$10^{-6.5}$ (x = 1.00)	2 Point Probe AC	[29–31]
$Li_xMn_2O_4$	$10^{-4.5}$ (x = 0.90)	2 Point Probe AC	[38]
$LiCo_yMn_{2-y}O_4$	(2.3×10^{-4} (y = 0.1); (2.5×10^{-2} (y = 1):at RT	AC impedance	[39]
$LiNi_yMn_{2-y}O_4$	0−4.5 (y = 0, to 0.6): at RT	4 Point Probe DC	[40]
Li_xFePO_4	10^{-2}:x = 0.8(impurity:$Fe_2P_2O_7$)	2 Point Probe AC	[41]
$Li_{1-x}M_xFePO_4$(M = Zr, Nb, Mg)	10^{-3} (size: 30 nm, C content: 5 wt%)	2 Point Probe AC	[42]

In addition, these calculations found that the (010) surface in $LiFePO_4$ has the optimum structure for Li^+ insertion according to the approximation of numerical data. Obviously, ab initio methods through artificial modeling might be inapplicable for multiple phases and disordered amorphous structure calculations.

2.2. Electrical Position in Anode Materials

The electronic details of graphite were completely evaluated in the past decades. Graphite is an important electrode due to having a zero-band gap and exhibiting special phenomena during the influence of electrical fields [23,24]. Interlayer interactions in graphite are too low and, due to the large distance between these layers, easily allow Li ions to move between these sheets. In addition, these intercalations cause unique crystal and electronic situations. In amorphous carbons, as disorder appears, electrical conductivity considerably reduces. Since quantum calculations and ab initio methods are not able to analyze the electronic situation of amorphous structure in graphite, several models have been developed to predict electrical conductivity in graphite [43,44].

2.3. Conduction Evaluating in Electrolytes

A perfect electrolyte for LIBs has not yet been found. Obviously, solvent electrolytes are extremely common because of higher ionic conductivities. Although various electrolyte compounds have been analyzed as replacements, some of them do not exhibit acceptable ionic conductivity, at least 10^{-3} Scm^{-1}, in LIBs [45]. The importance of electrolytes is to create an ionic conduction among the electrolytes and anodic and cathodic electrodes. Therefore, the main concern in electrolyte investigation is understanding how to increase ionic conductivity [46–48]. During the dissolving of cathode material salts in $LiPF_6$ as an important electrolyte, cathode ions (Li^+) and anions such as PF_6^- are produced. Since the

dissociation of the salt is relevant to dialectical conditions such as the constant of the solvent, when a high dielectric constant is present, strong solvating occurs [49]. Consequently, large anions of any salts, via high conductivity and solubility, can be properly distributed due to their negative charges.

2.4. Solid-State Electrolytes (SSEs)

SSEs have several advantages compared to liquid electrolytes, such as a simple design, suitable sealing, resistance to pressure and any vibrations or explosions under high temperatures, wide electrochemical stability, and better safety [50–52]. The important disadvantage of these types of electrolytes is lower ionic conductivity. The ionic conductivities of several solid-state electrolytes are listed in Table 3 [53–66]. The ion movement of gelled macromolecules and polymers containing high solubility is considerably different from that in crystalline materials [67–74]. Solid electrolytes fabricated in semiconductors have also been used widely as an important ingredient of solid-state micro batteries. Moreover, inorganic elements used in solid-state electrolytes often consist of rare metals such as Ge, Ti, Sc, In, Lu, La and Y that are too expensive [75]. Because of the mentioned problems for using solid-state electrolytes, only gel polymer electrolytes have been applied as commercial fabrications in markets [76].

Table 3. Ionic conductivity of various non-solid and SSEs.

Salt	Solvent	Ionic Conductivities (Scm^{-1})	Reference
Solid-state electrolytes (SSEs)			
Wet polymer	-	8.5×10^{-7} (LiPF6 6 wt% in PVdF)	[53]
Gel polymer	-	7.8×10^{-2} (at 25 °C)	[54]
Plastic crystal	-	1×10^{-4} (6%), 5×10^{-3} (12%):LiBF4	[57]
Crystalline (perovskite)	-	1.0×10^{-3} (x = 0, 0.2)	[58]
Crystalline (NASICON)	-	6.5×10^{-5}(at 200 °C)	[59]
Crystalline (thio-LISICON)	-	4.3×10^{-5} (x = 0)	[60]
Crystalline (Garnet)	-	5.2×10^{-4}	[62]
Glass (LiPON)	-	1.8×10^{-6} to 7.7×10^{-7}	[63]
Composite (glass + polymer)	-	1.2×10^{-3} (dry process)	[65]
Glass-ceramics	-	$1.\ 3 \times 10^{-8}$	[66]
Solvent electrolytes			
$LiClO_4$	PC	5.5	[77]
$LiAsF_6$	EC/DMC	8.5	[78]
$LiBF_4$	EC/DMC	11.3	[79]
$LiPF_6$	EC/DMC	10.5	[80]

Since the electrolyte material has a good Li^+ conductivity and is also electrochemically properly mobile, it must tolerate volume changes in both electrodes. In other words, Li^+ should tolerate the flux along cracks that causes glassy materials such as polycrystalline films to form leakage paths. Electrical measurements by Yu have demonstrated potentials up to 5.6 V in stable LiPON films in contact with lithium metal and the cathode [81] (Table 3). Since the ionic conductivity of LiPON is too low, this electrolyte is usually useful only in a 'thin film' configuration with solid electrolyte layer thicknesses around ~1000 nm. The thin film construction of batteries employing LiPON electrolyte limits overall capacity and therefore limits commercial application to small medical and MEMS devices. Fabrication of the LiSICON structure has been performed to create a 3D rigid framework for moving alkali ions through internal spaces. LiSICON electrolytes are made based on the formula $LixM_2M'_3O_{12}$, where M and M′ are generally metals and represent metal ions containing octahedral and tetrahedral coordination to the O_2^- ions such as $Li_8Mg_2Si_3O_{12}$ [82].

3. Materials and Methods

3.1. Ball Milling

Recently, several manufacturing techniques have been developed to prepare solid electrolytes, the most well-known being SSE, which is obtained by a high conductivity melt quenching method. During the preparation of SSE, an ionic conductivity of approximately 10^{-2} cm^{-1} was obtained and found to have suitable electrochemical stability [83]. Although there are different methods for fusion systems, the cooling method is one of the most important cases in that can be applied as an example of the usual method. In this way, the powders are first pressed through a suspension in a carbon-coated quartz tube and then vacuum sealed to obtain an ampoule of these materials. To prepare the glass substrate, the bulb is heated to 750 °C for half a day to obtain a single phase and uniform shape. Later, the temperature of the quenched material must be reduced with cold water to produce a solid solution. It is notable that for the crystallization of solutes, the bulb should be heated to 750 °C for half a day, and then the product can be kept for about two days at a certain temperature to promote nucleation and crystal growth. [84]. Figure 1 shows a general diagram of different phases containing 75% Li_2S with 25% P_2S_5 [84].

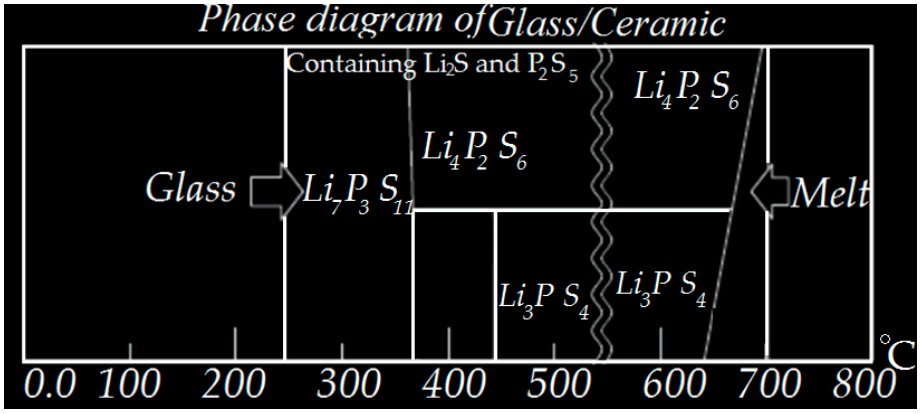

Figure 1. XRD of crystals glass showing a general phase diagram of the 75% Li_2S with %25P_2S_5.

Recently, ball milling methods have investigated the production of ultrafine amorphous at 298 K. The ideal powders are suitable for achieving large ionic conductivities and are also used to achieve the best contact between electrolytes and electrodes in SSE [85,86]. Ball milling probably also causes increased textural properties due to amorphous compounds, which are extracted using melt quenching techniques [87,88]. Ball-milled amorphous powders (BMAPs) are sometimes heated strongly to obtain crystalline units capable of higher conductivity compared to previous powders [89,90]. HEBM, which stands for high-energy ball milling, is an ideal technology for creating amorphous materials, and both contain the same concepts of pre-peel alloys using crushing technology. HEBM is generally carried out using shaker mills where the rotation takes place on a fixed axis. Although a high energy essentially causes a high-attrition grinding motion with the consideration of certain elements and proper control, the chambers rotating on a primary disk can be set at a selective speed. Since during grinding the compounds are alternately flattened, crushed, and welded, the steel balls trap certain particles between their surfaces. These impacts with enormous energies can severely destroy the molecules, reshape them atomically, and eliminate unusual surfaces and other structural defects [91,92]. Furthermore, the deforming and cracking of composites results in a progressive decrease in particle size and leads to significantly lower diffusion distances and temperatures [93–95]. BMAP is generally very stable and has stronger chemical interactions, which allows novel chemical reactions to be carried out while forming different nanostructures in our experiments. The behavior of hot milled electrolytes (BMEs) is confirmed by their excellent conductivity and solid electrolyte forming effects. For example, scientists have shown that heating ball-milled materials

beyond their glass transition temperature can lead to highly conductive crystalline solid electrolytes [96].

3.1.1. Cryogenic Milling/Grinding and Jet Milling

Cryogenic grinding is another technology that has many advantages, including temperature control and mechanical control of grinding by cooling or quenching the compound at low temperatures to reduce the particle size of 'soft' materials. Jet milling is also another method without any grinding system, but it works with near-sonic-speed jets. This technique is usually applied to reduce size reduction. Volume reduction and material mixing are the results of high-speed collisions among particles of the same processing material.

3.1.2. Single-Step Ball Milling (SSBM)

Although SSBM has advantages such as saving time and being efficient, its performance improvement compared to ball milling followed by heat treatment is not significant.

In addition, although ball milling followed by heat treatment has been shown to be effective, several steps of this process are time consuming and inefficient and should be modified. It is important to note that heat treatment typically produces glass-ceramic materials with larger particle size whose morphology may not be desirable for use in all-solid-state Li-ion batteries. A single-step ball milling (SSBM) procedure is proposed in this work in which ball milling and heat treatment are carried out simultaneously. Through this work, we will report the glass-ceramic binary system xLi_2S (100-x) P_2S_5 produced by the SSBM process in terms of structural and electrochemical properties.

3.2. Experimental

3.2.1. Preparation of P_2S_5, TiS_2, and Li_2S

Necessary and sufficient experiments were performed, as Li_2S (Sigma -Aldrich, 99%, Hamburg, Germany) and P_2S_5 (Sigma-Aldrich, 99%, Hamburg, Germany) were applied as initial compounds for mechanical ball milling through using stoichiometry concentrations with the proper fractions of zirconia: exactly one gram with two zirconia balls (1 × 10 mm, 1 × 13 mm in diameter) for grinding. Energy ball milling took place for 24 h in a glove box containing Argon gas at a temperature controller around 60 °C (Spex2000, Jiangsu, China). Ball-milled vials were alternatingly turned on and turned off to drive the temperature towards reaching the vial temperature. A perfect correlation was observed between the ambient vial temperature and that of the vials due to milling without pausing. In addition to maintaining room temperature, the vials were frequently milled in 40 min intervals. All prepared materials from ball milling at room temperature were amorphous and their conductivity values were confirmed through previous experimental values [85,86,90]. In this work, we changed the amorphous materials into pellets 15 mm in diameter and 0.8 mm thick in a titanium die through cold pressing (5 metric tons). The product samples were characterized through X-ray diffraction using Cu-Kα radiation and were sealed in an air-isolated aluminum box with beryllium vents, then fixed to the X-ray diffraction meter (PanAlytical PW3830 X-Ray, London, UK). The diffraction values were evaluated for all morphological structures as well as unique materials between 15 and 45 degrees. The ionic conductivities were calculated by AC impedance spectroscopy (Solartron 1280 C, München, Germany) for all SSBM samples. The weighed composites were then cold pressed using 10 tons/metric pressures to prevent the lithium electrode plates from being pressed to both sides of the pellet at 1 metric ton. The impedances of selected cells were calculated from 25 MHz to 110 mHz at 298 K and the conductivities were measured using complex impedance analysis. For providing TiS_2, several steps were accomplished as follows: 1. TiS_2 (Sigma-Aldrich, 99%, Hamburg, Germany) was ball milled in a 120 mL agate vial at a net weight of 600 mg. 2. Large-ball-milled (LBM) samples were produced via 8 agate balls (8 mm diameter) and small-ball-milled (SBM) composites with 45 agate balls (5 mm diameter) used for grinding. Ball milling took place for 3 h for large-ball-milled material

and 6 h for small-ball-milled products in an argon gas before the composites were used without further modification.

3.2.2. Preparation of Anode Materials

The anode electrode was made through a combination of crystalline nano-silicon (n-Si) powder (50–100 nm, Sigma-Aldrich, Hamburg, Germany) and bulk silicon (B-Si) powder (1–45 µm, Alfa Aesar brand of chemicals), solid-state electrolyte (SE) 76.0 Li_2S% -24.0P 2S 5% provided from ball milling methods, and also multi-walled-carbon-nanotubes (NC7000, Namur, Belgium) at a weight ratio of 1:6:1, respectively. We applied a conductive additive due to the increased contact surface (400 m^2g^{-1}) compared to acetylene black (65 m^2g^{-1}) (Figure 2A,B) and thus observed an acceptable increase in conductivity in our system. Double-layer pellets were produced by compressing 1 milligram of electrode material on top of 200 milligrams of SSE powder via five metric tons. Finally, the lithium sheet was pressed with SSE using one metric ton. A schematic diagram of the SSE-LIB cell can be seen in Figure 2C. All experiments and evaluations were performed in a poly-aryl-ether-ketone (PEEK) chip (I = 1.4 cm) and were also performed in an Ar-filled glove box with Ti metal rods as current collectors. Galvano/static measurement of charge-discharge cycling was performed for several items at a fixed density of 110 mAg^{-1} at 298 K using an Arbin BT2000 galvanostat. The product samples were characterized through X-ray diffraction using Cu-. Kα radiation and were sealed in an air-isolated aluminum box with beryllium vents and fixed on an X-ray diffraction meter (PanAlytical PW3830 X-Ray, London, UK).

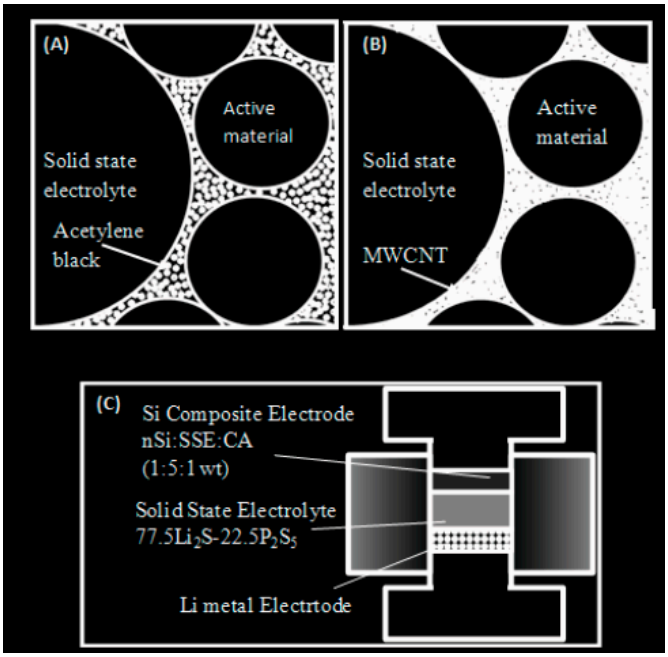

Figure 2. (**A**) Anode electrode containing acetylene black. (**B**) Multi-wall carbon nanotubes in anode. (**C**) Solid-state lithium battery including titanium.

3.2.3. Preparation of Cathode Materials

An important problem of SSE-LIBs is the difficulty of creating a suitable electrode–electrolyte interaction. In sulfide-based SSE-LIBs, high interfacial resistances among the cathode composite materials and the solid electrolyte have been seen during the initial charging process of $LiCoO_2$ as an effective cathode material. It is obvious that the high resistance is related to the destroying of the interface between the $LiCoO_2$ and the Li_2S-P_2S_5 solid electrolyte [97]. There are two ways of overcoming this problem: 1, using electrolyte additives for enhancing ionic conductivities and fixing the electrolyte in contact with the electrode, 2, creating a favorable electrode–electrolyte interface by interfacial modification. It has been confirmed that by using compounds such as GeS_2 and SiS_2 to create the network

of the Li_2S-P_2S_5 system, not only can higher conductivities for SSE be gained, but a better stability of the electrode–electrolyte system can also be formed [98]. Due to the second crystal structure, the elements with large ionic radius and high polarizability can be used, which consequently cause an increasing situation of mobility and conducting ions towards improving the solid crystal of the electrolytes [99]. These types of additive materials can decrease the large chemical potential difference among the components of a sulfide electrolyte as well as an oxide electrode. Creating a suitable electrode–electrolyte system by the optimization of cathode material surfaces has also confirmed an effective reduction in the resistance through coatings of $Li_4Ti_5O_{12}$ on $LiCoO_2$ particles [100]. In addition, a novel molecule was discovered, $Li_4Ti_5O_{12}$, that can prevent dissolution [101]; coating by this molecule prevents the diffusion of the $LiCoO_2$ inside the electrolyte. In this study, we investigated the mentioned additives in solid electrolytes to increase the stability of electrode materials with electrolytes. $GeSe_2$ was used as a second network to improve the electrical conductivity and stabilize the SSE in our work, because sulfur is used as an additive to help stabilize the electrolyte for the high voltage in cathode electrodes.

Li_2S-P_2S_5 as an SSE provided through ball milling as well as milling outputs in amorphous compounds elevated temperature conductivity values to 8.99×10^{-3} S cm^{-1} and 9.93×10^{-4} S cm^{-1}, respectively. Cathode composite materials were mixed using both ball-milled and non-ball-milled titanium sulfide powders and SSE at a ratio of 2:3, respectively. For composites containing acetylene black (Alfa-Aesar, 60% compressed) as a conductive additive, a ratio of 15:20:2 was applied for three compounds consisting of TiS_2, solid electrolyte, and acetylene black, respectively. Battery pellets were made by cold pressing (6 metric tons) and 12 mg of the composite cathode electrode above 150 mg of SE for 5 min. Li foil (Alfa-Aesar, 0.70 mm thick) was then attached to the SSE surface at 3 metric tons. All pressing and testing products were accomplished in a polyaryletheretherketone (PEEK) mold (I = 1.5 cm) with titanium rods as current collectors for both electrodes in an Ar-filled glove box.

3.2.4. Electrolyte Fabrication

Li_2S-GeS_2-P_2S_5 SSE was created using the SSBM method [102,103]. Reagent-grade powders of Li_2S (Aldrich, 99.0%), P_2S_5 (Aldrich, 99%), and GeS_2 (City Chemical, 99.0%) were consumed as initial products. Suitable amounts of composites were mixed into a zirconia vial (Spex) at a net weight of 1.5 g with two zirconia balls for grinding. HEBM (Spex8000) tool was selected and kept for 15 h in an Ar-filled dry box. The heat action of SSBM:SSE powders was accomplished through the initial mixing of sulfur and SSE powders and pelletizing the powders at 6 metric tons in a stainless steel die (I = 1.5 cm) with 500 mg of initial compounds. The provided pellets were fixed in a sealed glass container and were heated to 250 °C for 15 h. Both Li_2S-$GeSe_2$-P_2S_5 and $Li_{4x}Ge_{1-x}P_xS_{2(1+x)}Se_{2(1-x)}$ electrolytes were prepared similarly with $GeSe_2$ (Stream, 99.9%) and instead used temperatures of 240 °C, 350 °C, and 450 °C.

3.2.5. Electrode Fabrication with Bilayer Electrolyte

Cathode materials were provided through mixing $LiCoO_2$ powder (Sigma-Aldrich) as the active material, SSE Li_2S-GeS_2-P_2S_5 powder for quick conduction of lithium, and acetylene black (Alfa, 55% compressed) for electron conduction at a weight ratio of 25:50:2, respectively. Double-layered pellets were made through a 120 mg hand pressing of Li_2S-$GeSe_2$-P_2S_5 or Li_2S-GeS_2-P_2S_5 SSE over an 80 mg hand-pressed layer of 69.5 Li_2S -19.5 P_2S_5 SSE created using the SSBM method. Then, a 12 mg layer of the cathode compounds was carefully diffused over the Li_2S-$GeSe_2$-P_2S_5 or Li_2S-GeS_2-P_2S_5 solid electrolyte and the cell was pelletized through cold pressing for 6 min. All experiments were performed in an argon-gas-filled glove box. Galvanostatic charge-discharge cycling occurred at initial cycle cut off voltages of 4.5 and 2.0 V at a 45 μA cm^{-2} current at 298K using an Arbin BT2000. Schematic diagrams for the Li/SSE/$LiCoO_2$ and AC impedance cells can be seen in Figure 3.

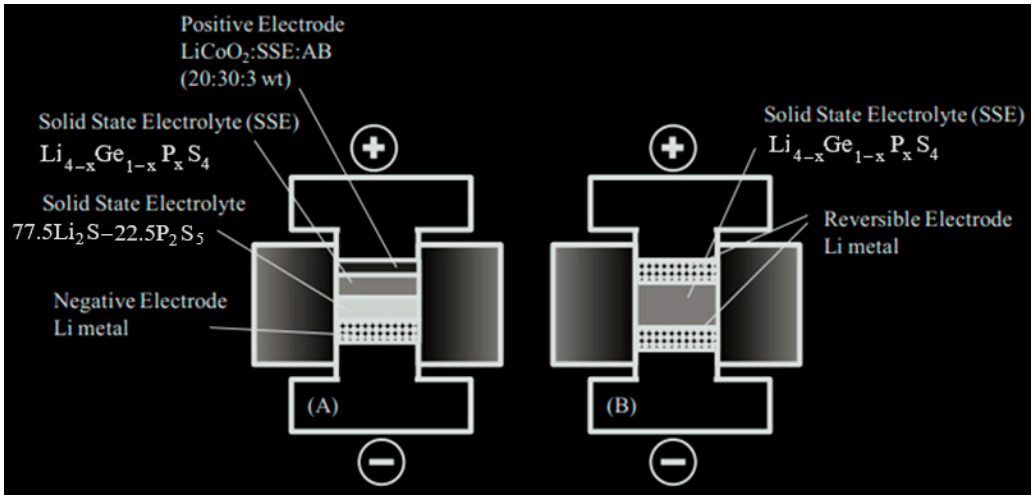

Figure 3. Titanium test with Li_2S–GeS_2–P_2S_5 SSE, (**A**) solid electrolyte battery, and (**B**) conductivity tester.

4. Results and Discussion

4.1. Characterization

Figure 4 exhibits the XRD spectrum of several glass-ceramic morphologies in the combination of 65 < x < 85 for [$xLi_2S_{(100-x)}P_2S_5$]. A sharp peak can be seen among all items denoting the crystalline composition prepared under the SSBM method. For x = 76.5 and x = 79, electrolytes with sharp diffraction peaks are observed near 24.9 and 30.5 due to excess Li_2S content in their composition [104].

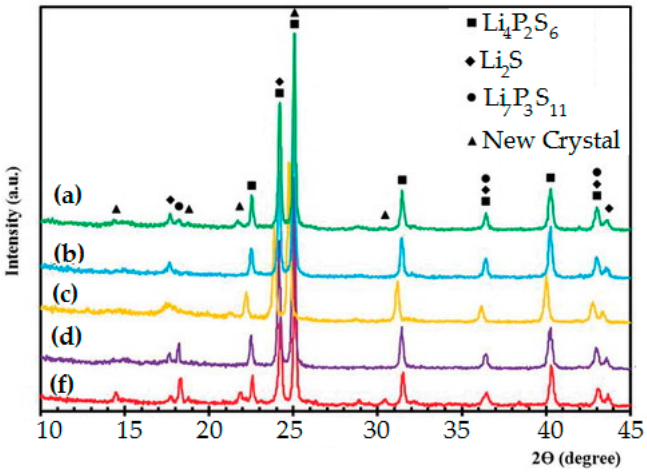

Figure 4. XRD patterns for all tested electrolytes, (a) Li_2S, (b) P_2S_5, (c) x = GeS_2, (d) x = 64, (f) x = 76.

The diffraction patterns for SSBM composites denote a linearly increasing intensity of crystalline peaks up to x = 76.5, at which point only the Li_2S peaks intensify for x = 79. A new crystalline pattern, identical to that of the thio-LISICON II analog, can be seen through positioned peaks among the materials ranges [104]. The specific behavior of composites such as the low melting temperature of P_2S_5 might be a reason for the crystallization of these compounds during SSBM. Measurements were accomplished from the cathodic and then the anodic situations up to 4.5 V vs. Li^+/Li and down to 0.5 V vs. Li^+/Li. No reactions were observed in these voltammograms except for the lithium deposition ($Li^+ + e \rightarrow Li$) and dissolution ($Li \rightarrow Li^+ + e$) reactions between 0.5 and 0.6 V up to 4.5 V vs. Li^+/Li. This suggests that the SSBM composites have a wider electrochemical window than 4.5 V [105].

4.2. Conductivities

Figure 5 exhibits the details of a conductive situation according to values that were measured from amorphous and SSBM ceramic glasses. Through two-step testing, increasing conductivities over glass electrolytes appeared due to the formation of unique crystalline structures [26]. In other words, the enhancement in conductivity by the crystallization of sulfide-based glass solid electrolytes appeared due to the crystalline phase, which is produced during the ball milling process. In addition, the LISICON phase of $Li_{(4-x)}Ge_{(1-x)}P_xS_4$ ($0.5 < x < 0.9$) with high conductivities was created through monoclinic superstructure [41]. We predicted that enhancements of conductivities are caused mostly by SSBM when they are around one or two orders of magnitude compared to other glass electrolytes as well as higher than these values for glass-ceramics, which were created using two heating steps [26].

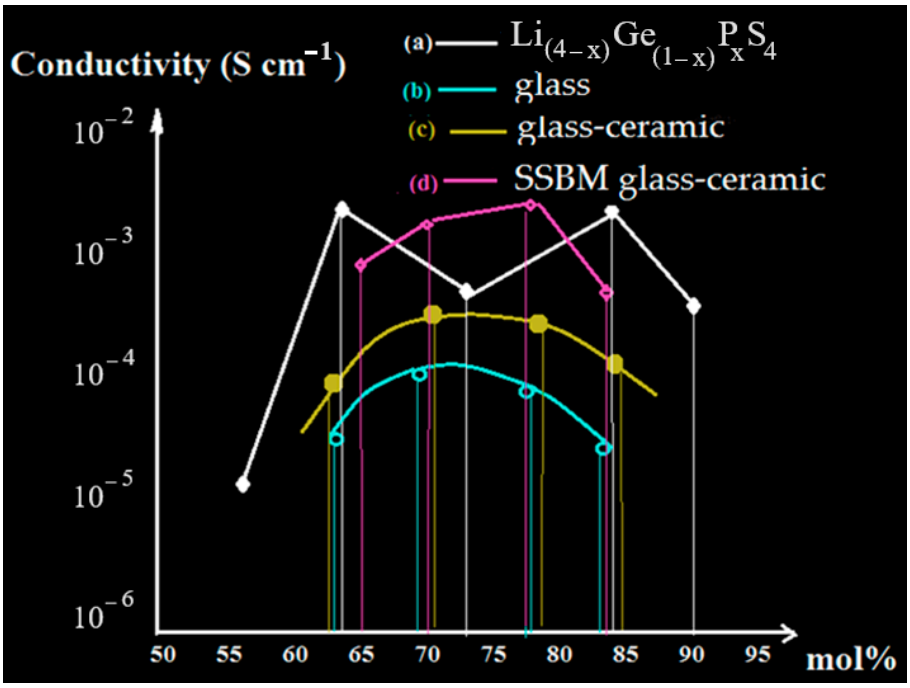

Figure 5. (a) Conductivity map for $Li_{(4-x)}Ge_{(1-x)}P_xS_4$; (b) glass, (c) glass-ceramic, (d) SSBM glass-ceramic.

Conductive Additive Modification by MWCNTs

Multiwall carbon nanotubes (MWCNTs), due to their unique one-dimensional structure and tubular structure, high electrical and thermal conductivities, and extremely large surface area, have been considered as ideal additive materials to improve the electrochemical characteristics of the anodes and cathodes of Li-ion batteries. A recent development of electrode materials for LIBs has been driven mainly by hybrid nanostructures consisting of Li storage compounds and MWCNTs. The electrochemical performance of LIBs affected by the presence of MWCNTs in terms of energy and power densities, rate capacity, cyclic life and safety are highlighted in comparison with those without or containing other types of carbonaceous materials. Figure 6 exhibits the extra efficiency of the conductive additive modification including n-Si cells using MWCNT at three temperatures (298, 300, 302 K) under galvanic-static charge/discharge cycling between 1.5 V and 5 V (vs. Li/Li^+). It is usual to show the specific capacities based on the mass of the active materials such as nano-Si in the anode. In addition, the lithium interaction capacity of MWCNTs can considerably help the total capacities of the anode materials. Consequently, the capacities of the conductive additives were gained in the cell using several amounts of the MWCNTs as the active material. The specific capacities of these amounts in the anode were then estimated from the data for the corresponding capacity of nano-Si according to the use of

MWCNT amounts. We found a considerable enhancing of the specific surface area of the MWCNTs for flexion for maintaining the electrical contact with the nano-Si particles upon cycling [7]. This test confirms that solid-state lithium batteries using nano-Si and MWCNTs as a conductive additive maintain a considerable capacity and amazingly exhibit higher efficiency compared with those batteries that do not use nano-Si. MWCNTs were found to improve cycling capacity in all-solid-state lithium batteries over acetylene black as a conductive additive.

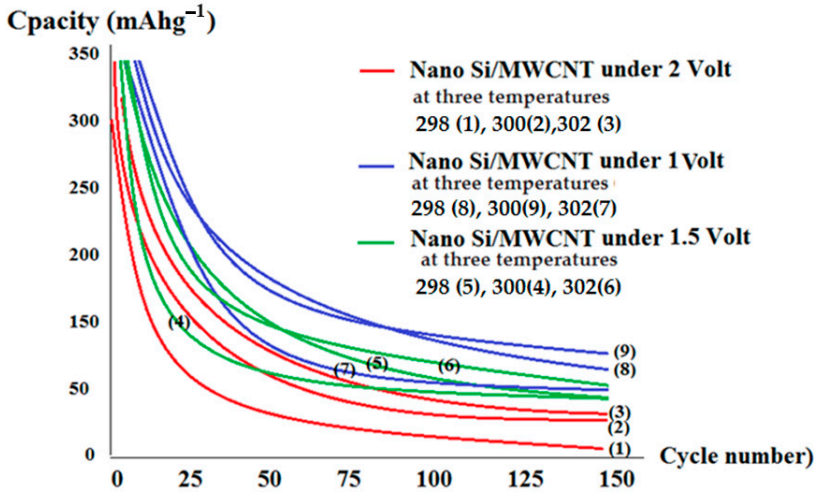

Figure 6. Comparison showing superior performance of MWCNT as a conductive additive for all solid–state lithium batteries over acetylene black in different voltages and three temperatures.

4.3. Liquid vs. Solid

The battery cell was cycled between 0 and 150 and voltages between 1.5 V to 5 V versus Li^+/Li at a current density of 500 mAg^{-1} at room temperature. The first discharge and charge values of nano-Si were found to be various values based on Figure 7 from A to H, respectively. During the first cycle (Figure 7A), the potential quickly drops to 3.2 V, then gradually reaches 2.4 V. Figure 7B compares the cycling performance of solid-state and liquid electrolyte systems using nano-Si; the charge capacity of the solid glass-ceramic electrolyte system reduces from 250 to 50 mAhg-1 within 0–50 cycles (Figure 7C). The nano-Si in solid-state electrolyte demonstrated a capacity retention of 71.5% after 50 charge/discharge cycles in these ranges of voltages (Figure 7D). In contrast, the nano-Si in the conventional liquid electrolyte cell displayed a maximum of 20% capacity retention (Figure 7E). This difference is related to the amount of expansion during Li accumulation, because the amount changes of Li-Si permit Si absorption in lithium through a liquid electrolyte compared with solid electrolytes (Figure 7F).

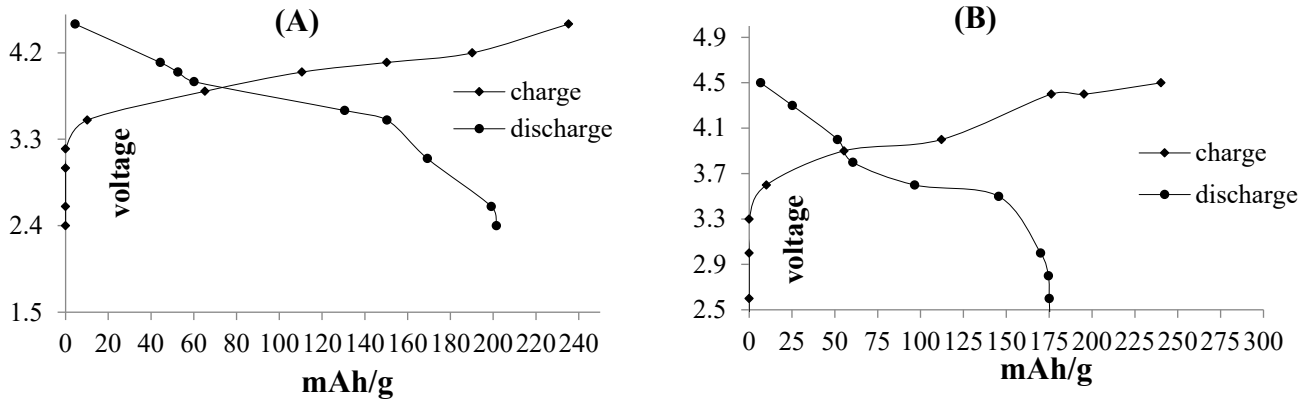

Figure 7. *Cont.*

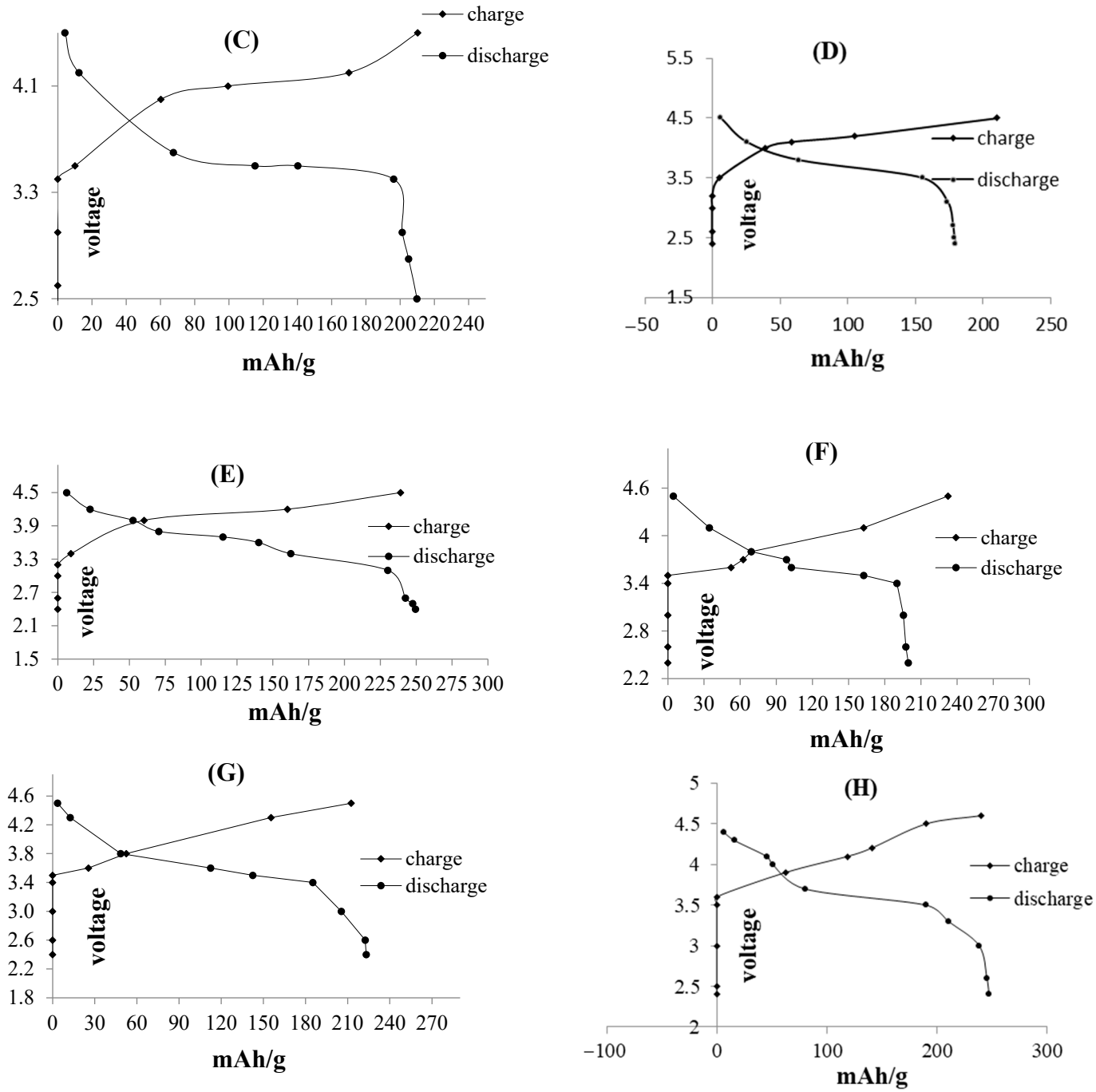

Figure 7. Charge–discharge curves of all-solid-state cell fabricated with n-Si as anode material by different voltage ranges. (**A**–**F**) compare the cycling performance of solid state and liquid electrolyte systems using nano-Si. (**G**,**H**) exhibit the charge-discharge performance of ion cells, tested with lithium phosphorus oxy-nitride (LIPON) and lithium super-ionic conductor (SILICON) solid electrolyte, respectively.

5. Conclusions

Here, we found that electrodes composed of silicon rods control the electrolytes of LIBs because they can provide more stability with optimized crushing, as well as creating an appropriate lifespan and sufficient Coulomb efficiency. The simplicity of the SSBM process and high ionic conductivity of SSBM samples make the SSBM method superior for the development of SSE for all-solid-state battery production. Through this work, we confirmed, using the glass-ceramic electrolytes produced by the SSBM technique, that

silicon nanoparticles can be used as the anode material in all-solid-state Li-ion batteries. This work also confirms that solid-state lithium batteries using nano-Si and MWCNTs as a conductive additive maintain a considerable capacity and, amazingly, exhibit higher efficiency compared to those batteries without using nano-Si. As a result, MWCNTs can improve cycling capacity in all-solid-state lithium batteries over acetylene black as a conductive additive for any further research.

Author Contributions: Conceptualization, M.M. and F.M.; methodology, M.M.; software, F.M.; validation, M.M.; formal analysis, M.M. and F.M.; investigation, M.M. and F.M.; resources, M.M.; data curation, M.M.; writing—original draft preparation, F.M.; writing—review and editing, F.M.; visualization, M.M. and F.M.; supervision, M.M.; project administration, M.M. All authors have read and agreed to the published version of the manuscript.

Funding: This research received no external funding.

Data Availability Statement: Data available on request due to restrictions (e.g., privacy, legal or ethical reasons).

Conflicts of Interest: The authors declare no conflicts of interest.

References

1. Zhao, W.; Yi, J.; He, P.; Zhou, H. Solid-State Electrolytes for Lithium-Ion Batteries: Fundamentals, Challenges and Perspectives. *Electrochem. Energ. Rev.* **2019**, *2*, 574–605. [CrossRef]
2. Flamme, B.; Rodriguez Garcia, G.; Weil, M.; Haddad, M.; Phansavath, P.; Ratovelomanana-Vidala, V.; Chagnes, A. Guidelines to design organic electrolytes for lithium-ion batteries: Environmental impact, physicochemical and electrochemical properties. *Green Chem.* **2017**, *19*, 1828. [CrossRef]
3. Cheng, X.; Pan, J.; Zhao, Y.; Liao, M.; Peng, H. Gel Polymer Electrolytes for Electrochemical Energy Storage. *Adv. Energy Mater.* **2017**, *8*, 1702184. [CrossRef]
4. Baskoro, F.; Wong, H.Q. Strategic Structural Design of a Gel Polymer Electrolyte toward a High Efficiency Lithium-Ion Battery. *ACS Appl. Energy Mater.* **2019**, *2*, 3937–3971. [CrossRef]
5. Alipoori, S.; Mazinani, S.; Aboutalebi, S.H.; Sharif, F. Review of PVA-based gel polymer electrolytes in flexible solid-state supercapacitors: Opportunities and challenges. *J. Energy Storage* **2020**, *27*, 101072. [CrossRef]
6. Cai, H.; Chen, Z.; Guo, S.; Ma, D.; Wang, J. Polyacrylamide gel electrolyte for high-performance quasi-solid-state electrochromic devices. *Sol. Energy Mater. Sol. Cells* **2023**, *256*, 112310. [CrossRef]
7. Wang, C.; Zhang, D.; Yue, J.; Zhang, X.; Wu, Z.; Zhang, T.; Chen, C.; Fei, T. Optical Waveguide Sensors for Measuring Human Temperature and Humidity with Gel Polymer Electrolytes. *ACS Appl. Mater. Interfaces* **2021**, *13*, 60384–60392. [CrossRef]
8. Kim, K.J.; Hyeon, J.S.; Kim, H.; Mun, T.J.; Haines, C.S.; Li, N.; Baughman, R.H.; Kim, S.J. Enhancing the Work Capacity of Electrochemical Artificial Muscles by Coiling Plies of Twist-Released Carbon Nanotube Yarns. *ACS Appl. Mater. Interfaces* **2019**, *11*, 13533–13537. [CrossRef]
9. Yang, H.X.; Liu, Z.K.; Wang, Y.; Li, N.W.; Yu, L. Multiscale Structural Gel Polymer Electrolytes with Fast Li+ Transport for Long-Life Li Metal Batteries. *Adv. Funct. Mater.* **2023**, *33*, 2209837. [CrossRef]
10. Sohn, J.-Y.; Choi, J.H.; Kim, P.-W.; Hwang, I.T.; Shin, J.; Jung, C.-H.; Lee, Y.-M. In-situ preparation of chemically-crosslinked polyvinylpyrrolidone gel polymer electrolyte for lithium ion battery via room-temperature electron beam-induced gelation. *Radiat. Phys. Chem.* **2023**, *211*, 111047. [CrossRef]
11. Wang, X.; Hao, X.; Xia, Y.; Liang, Y.; Xia, X.; Tu, J. A polyacrylonitrile (PAN)-based double-layer multifunctional gel polymerelectrolyte for lithium-sulfur batteries. *J. Membr. Sci.* **2019**, *582*, 37–47. [CrossRef]
12. Zhou, Z.; Pei, X.; Zhang, T.; Wang, L.; Hong, J.; Lu, Y.; He, G. A Gel Polymer Electrolyte with 2D Filler-reinforced for Dendrite Suppression Li-Ion Batteries. *Electroanalysis* **2023**, *35*, 2200306. [CrossRef]
13. Dennis, J.O.; Shukur, M.F.; Aldaghri, O.A.; Ibnaouf, K.H.; Adam, A.A.; Usman, F.; Hassan, Y.M.; Alsadig, A.; Danbature, W.L.; Abdulkadir, B.A. A Review of Current Trends on Polyvinyl Alcohol (PVA)-Based Solid Polymer Electrolytes. *Molecules* **2023**, *28*, 1781. [CrossRef]
14. Marchiori, C.F.N.; Carvalho, R.P.; Ebadi, M.; Brandell, D.; Moyses Araujo, C. Understanding the Electrochemical Stability Window of Polymer Electrolytes in Solid-State Batteries from Atomic-Scale Modeling: The Role of Li-Ion Salts. *Chem. Mater.* **2020**, *32*, 7237–7246. [CrossRef]
15. Shaplov, A.S.; Marcilla, R.; Mecerreyes, D. Recent Advances in Innovative Polymer Electrolytes based on Poly (ionic liquid)s. *Electrochim. Acta* **2015**, *175*, 18–34. [CrossRef]
16. Cho, Y.G.; Hwang, C.; Cheong, D.S.; Kim, Y.-S.; Son, H.-K. Gel/Solid Polymer Electrolytes Characterized by In Situ Gelation or Polymerization for Electrochemical Energy Systems. *Adv. Mater.* **2019**, *31*, 1804909. [CrossRef] [PubMed]
17. Peng, S.; Liu, S.; Sun, Y.; Xiang, N.; Jiang, X.; Hou, L. Facile preparation and characterization of poly(vinyl alcohol)-NaCl-glycerol. *Eur. Polym. J.* **2018**, *106*, 206–213. [CrossRef]

18. Shi, S.; Peng, X.; Liu, T.; Chen, Y.-N.; He, C.; Wang, H. Facile preparation of hydrogen-bonded supramolecular polyvinylalcohol-glycerol gels with excellent thermoplasticity and mechanical properties. *Polymer* **2017**, *111*, 168–176. [CrossRef]
19. Sun, Y.; Xiang, N.; Jiang, X.; Hou, L. Preparation of high tough poly(vinyl alcohol) hydrogel by soaking in NaCl aqueous solution. *Mater. Lett.* **2017**, *194*, 34–37. [CrossRef]
20. Di, X.; Ma, Q.; Xu, Y.; Yang, M.; Wu, G.; Sun, P. High-performance ionic conductive poly(vinyl alcohol) hydrogels for flexible strain sensors based on a universal soaking strategy. *Mater. Chem. Front.* **2021**, *5*, 315–323. [CrossRef]
21. Callister, W.D., Jr. *Materials Science and Engineering: An Introduction*, 4th ed.; John Wiley & Sons: Hoboken, NJ, USA, 1997; pp. 796–801.
22. Novoselov, K.S.; Geim, A.K.; Morozov, S.V.; Jiang, D.; Zhang, Y.; Dubonos, S.V.; Grigorieva, I.V.; Firsov, A.A. Electric field effect in atomically thin carbon films. *Science* **2004**, *306*, 666–669. [CrossRef] [PubMed]
23. Partoens, B.; Peeters, F.M. From graphene to graphite: Electronic structure around the *K* point. *Phys. Rev. B* **2006**, *74*, 075404. [CrossRef]
24. Hess, M.; Lebraud, E.; Levasseur, A. Graphite multilayer thin films: A new anode material for Li-ion microbatteries synthesis and characterization. *Power Sources* **1997**, *68*, 204–207. [CrossRef]
25. Segall, B. Energy bands of aluminum. *Phys. Rev.* **1961**, *124*, 1797–1806. [CrossRef]
26. Kemp, J.P.; Cox, P.A. Electronic structure of $LiCoO_2$ and related materials; photoemission studies. *Phys. Condens. Matter* **1990**, *2*, 9653–9667. [CrossRef]
27. Shi, S.; Ouyang, C.; Lei, M.; Tang, W. Effect of Mg-doping on the structural and electronic properties of $LiCoO_2$: A first-principles investigation. *Power Sources* **2007**, *171*, 908–912. [CrossRef]
28. van Elp, J.; Wieland, J.L.; Eskes, H.; Kuiper, P.; Sawatzky, G.A. Electronic structure of CoO, Li-doped CoO, and LiCOO2. *Phys. Rev. B* **1991**, *44*, 6090–6103. [CrossRef]
29. Ragavendran, K.; Nakkiran, A.; Kalyani, P.; Veluchamy, A.; Jagannathan, R. Nickel doped spinel lithium manganate–some insights using opto-impedance. *Chem. Phys. Lett.* **2008**, *456*, 110–115. [CrossRef]
30. Marzec, J.; Swierczek, K.; Przewoznik, J.; Molenda, J.; Simon, D.R.; Kelder, E.M.; Schoonman, J. Conduction mechanism in operating a LiMn2O4 cathode. *Solid State Ion.* **2002**, *146*, 225–237. [CrossRef]
31. Molenda, J.; Kucza, W. Transport properties of LiMn2O4. *Solid State Ion.* **1999**, *117*, 41–46. [CrossRef]
32. Shi, S.; Liu, L.; Ouyang, C.; Wang, D.S.; Wang, Z.; Chen, L.; Huang, X. Enhancement of electronic conductivity of $LiFePO_4$ by Cr doping and its identification by first-principles calculations. *Phys. Rev. B* **2003**, *68*, 195108-1–195108-5. [CrossRef]
33. Xu, Y.N.; Chung, S.Y.; Bloking, J.T.; Chiang, Y.M.; Ching, W.Y. Electronic structure and electrical conductivity of undoped $LiFePO_4$. *Electrochem. Solid State Lett.* **2004**, *7*, A131–A134. [CrossRef]
34. Takahashi, Y.; Kijima, N.; Tokiwa, K.; Watanabe, T.; Akimoto, J. Single-crystal synthesis, structure refinement and electrical properties of $Li_{0.5}CoO_2$. *Phys. Condens. Matter* **2007**, *19*, 436202–1–436202-12. [CrossRef]
35. Levasseur, S.; Ménétrier, M.; Delmas, C. On the Dual Effect of Mg Doping in $LiCoO_2$ and $Li_{1+\delta}CoO_2$: Structural, Electronic Properties, and ^{7}Li MAS NMR Studies. *Chem. Mater.* **2002**, *14*, 3584–3590. [CrossRef]
36. Carlier, D.; Ménétrier, M.; Delmas, C.J. ^{7}Li MAS NMR study of electrochemically deintercalated $Li_xNi_{0.30}Co_{0.70}O_2$ phases: Evidence of electronic and ionic mobility, and redox processes. *J. Mater. Chem.* **2001**, *11*, 594–603. [CrossRef]
37. Lala, S.M.; Montoro, L.A.; Abbate, M.; Rosolen, J.M. The negative and positive structural effects of Ga doping in the electrochemical performance of $LiCoO_2$. *Electrochim. Acta* **2005**, *51*, 7–13. [CrossRef]
38. Ramos Ferrer, P.; Mace, A.; Thomas, S.N.; Jeon, J.W. Nanostructured porous graphene and its composites for energy storage applications. *Nano Converg.* **2017**, *4*, 29. [CrossRef]
39. Molenda, J.; Swierczek, K.; Marzec, J.; Liu, R.S. Charge transport mechanism in $LiCoyMn_2-yO_4$ cathode material. *Solid State Ion.* **2003**, *157*, 101–108. [CrossRef]
40. Lazarraga, M.G.; Pascual, L.; Gadjov, H.; Kovacheva, D.; Petrov, K.; Amarilla, J.M.; Rojas, R.M.; Martin-Luengo, M.A.; Rojo, J.M. Nanosize $LiNi_yMn_2 - yO_4$ ($0 < y \leq 0.5$) spinels synthesized by a sucrose-aided combustion method. Characterization and electrochemical performance. *Mater. Chem.* **2004**, *14*, 1640–1647.
41. Kim, D.K.; Park, H.M.; Jung, S.J.; Jeong, Y.U.; Lee, J.H.; Kim, J.J. LiMnPO4: Review on Synthesis and Electrochemical Properties. *Power Sources* **2006**, *159*, 237–240. [CrossRef]
42. Zhou, F.; Cococcioni, M.; Marianetti, C.A.; Morgan, D.; Ceder, G. First-principles prediction of redox potentials in transition-metal compounds with LDA+*U*. *Phys. Rev. B* **2004**, *70*, 235121–1–235121–8. [CrossRef]
43. Ravagnan, L.; Piseri, P.; Bruzzi, M.; Miglio, S.; Bongiorno, G.; Baserga, A.; Casari, C.S.; Bassi, A.L.; Lenardi, C.; Yamaguchi, Y.; et al. Influence of Cumulenic Chains on the Vibrational and Electronic Properties of sp-sp2 Amorphous Carbon. *Phys. Rev. Lett.* **2007**, *98*, 216103-1–216103-4. [CrossRef]
44. Vishwakarma, P.N.; Subramanyam, S.V. Hopping conduction in boron doped amorphous carbon films. *J. Appl. Phys.* **2006**, *100*, 113702–1–113702-5. [CrossRef]
45. Brodd, R.J.; Huang, W.; Akridge, J.R. Advances in Lithium-Ion Batteries. *Macromol. Symp.* **2000**, *159*, 229–245. [CrossRef]
46. Chagnes, A.; Carré, B.; Willmann, P.; Lemordant, D. Guidelines to Design Electrolytes for Lithium-ion Batteries: Environmental Impact, Physicochemical and Electrochemical Properties. *Power Sources* **2002**, *109*, 203–213. [CrossRef]
47. Geoffroy, I.; Willmann, P.; Mesfar, K.; Carré, B.; Lemordant, D. Electrolytic characteristics of ethylene carbonate–diglyme-based electrolytes for lithium batteries. *Electrochim. Acta* **2000**, *45*, 2019–2027. [CrossRef]

48. Ding, M.S.; Jow, T.R. Evaluation of Fluorinated Alkyl Phosphates as Flame Retardants in Electrolytes for Li-Ion Batteries I. Physical and Electrochemical Properties. *J. Electrochem. Soc.* **2003**, *150*, A620–A628. [CrossRef]
49. Blint, R.J. Chemistry-Informed Machine Learning for Polymer Electrolyte Discovery. *Electrochem. Soc.* **1995**, *142*, 696–702. [CrossRef]
50. Ribes, M. *Thin Film Technology and Characterization: Their Use in Microionic Devices. Solid State Microbatteries*; James, R., Akridge, M.B., Eds.; Plenum Press: New York, NY, USA, 1990; pp. 41–58.
51. Wakihara, M. Recent developments in lithium ion batteries. *Mater. Sci. Eng. R* **2001**, *33*, 109–134. [CrossRef]
52. Zaghib, K.; Charest, P.; Guerfi, A.; Shim, J.; Perrier, M.; Striebel, K. Safe Li-ion polymer batteries for HEV applications. *Power Sources* **2004**, *134*, 124–129. [CrossRef]
53. Chiang, C.-Y.; Shen, Y.J.; Reddy, M.J.; Chu, P.P. Complexation of poly(vinylidene fluoride): LiPF6 solid polymer electrolyte with enhanced ion conduction in 'wet'form. *Power Sources* **2003**, *123*, 222–229. [CrossRef]
54. Kaneko, M.; Nakayama, M.; Wakihara, M. Lithium-ion conduction in elastomeric binder in Li-ion batteries. *Solid State Electrochem.* **2007**, *11*, 1071–1076. [CrossRef]
55. Egashira, M.; Todo, H.; Yosimoto, N.; Morita, M. Lithium ion conduction in ionic liquid-based gel polymer electrolyte. *Power Sources* **2008**, *178*, 729–735. [CrossRef]
56. Zhang, S.; Lee, J.Y.; Hong, L. Li^+ conducting 'fuzzy'poly (ethylene oxide)–SiO_2 polymer composite electrolytes. *Power Sources* **2004**, *134*, 95–102. [CrossRef]
57. Abouimrane, A.; Whitfield, P.S.; Niketic, S.; Davidson, I.J. Investigation of Li salt doped succinonitrile as potential solid electrolytes for lithium batteries. *Power Sources* **2007**, *174*, 883–888. [CrossRef]
58. Yang, K.Y.; Fung, K.Z.; Leu, I.C. Study on the structural change and lithium ion conductivity for the perovskite-type $LaAlO_3$–$La_{0.50}Li_{0.50}TiO_3$ solid solution. *Alloys Compd.* **2007**, *438*, 207–216. [CrossRef]
59. Savitha, T.; Selvasekarapandian, S.; Ramya, C.S.; Bhuvaneswari, M.S.; Hirankumar, G.; Baskaran, R.; Angelo, P.C. Structural and ionic transport properties of $Li_2AlZr[PO_4]_3$. *Power Sources* **2006**, *157*, 533–536. [CrossRef]
60. Kanno, R.; Hata, T.; Kawamoto, Y.; Irie, M. Synthesis of a new lithium ionic conductor, thio-LISICON–lithium germanium sulfide system. *Solid State Ion.* **2000**, *130*, 97–104. [CrossRef]
61. Tomita, Y.; Matsushita, H.; Kobayashi, K.; Maeda, Y.; Yamada, K. Substitution effect of ionic conductivity in lithium ion conductor, $Li_3InBr_{6-x}Cl_x$. *Solid State Ion.* **2008**, *179*, 867–870. [CrossRef]
62. Thangadurai, V.; Schwenzel, J.; Weppner, W. Tailoring ceramics for specific applications: A case study of the development of all-solid-state lithium batteries. *Ionics* **2005**, *11*, 11–23. [CrossRef]
63. Hamon, Y.; Douard, A.; Sabary, F.; Marcel, C.; Vinatier, P.; Pecquenard, B.; Levasseur, A. Influence of sputtering conditions on ionic conductivity of LiPON thin films. *Solid State Ion.* **2006**, *177*, 257–261. [CrossRef]
64. Kennedy, J.H.; Zhang, Z. Further Characterization of Sis2-Li2s Glasses Doped with Lithium Halide. *Electrochem. Soc.* **1988**, *135*, 859–862. [CrossRef]
65. Inada, T.; Takada, K.I.; Kajiyama, A.; Kouguchi, M.; Sasaki, H.; Kondo, S.; Watanabe, M.; Murayama, M.; Kanno, R. Fabrications and properties of composite solid-state electrolytes. *Solid State Ion.* **2003**, *158*, 275–280. [CrossRef]
66. Chowdari, B.V.R.; Rao, G.V.S.; Lee, G.Y.H. XPS and ionic conductivity studies on Li_2O–Al_2O_3–(TiO_2 or GeO_2)–P_2O_5 glass–ceramics. *Solid State Ion.* **2000**, *136–137*, 1067–1075. [CrossRef]
67. Ohta, N.; Takada, K.; Sakaguchi, I.; Zhang, L.; Ma, R.; Fukuda, K.; Osada, M.; Sasaki, T. $LiNbO_3$-coated $LiCoO_2$ as cathode material for all solid-state lithium secondary batteries. *Electrochem. Commun.* **2007**, *9*, 1486–1490. [CrossRef]
68. Ratner, M.A.; Shriver, D.F. Ion transport in solvent-free polymers. *Chem. Rev.* **1988**, *88*, 109–124. [CrossRef]
69. Papke, B.L.; Ratner, M.A.; Shriver, D.F. Conformation and ion-transport models for the structure and ionic conductivity in complexes of polyethers with alkali Metal Salts. *Electrochem. Soc.* **1982**, *129*, 1694–1701. [CrossRef]
70. Brandup, J.; Immergut, E.H.; Grulke, E.A.; Abe, A.; Bloch, D.R. (Eds.) *Solution Properties, Polymer Handbook*, 4th ed.; John Wiley and Sons: Hoboken, NJ, USA, 1999.
71. Le Nest, J.F.; Callens, S.; Gandini, A.; Armand, M. Additives for Solid Polymer Electrolytes: The Layered Nanoparticles. *Electrochim. Acta* **1992**, *37*, 1585–1588. [CrossRef]
72. Nishimoto, A.; Watanabe, M.; Ikeda, Y.; Kohjiya, S. High ionic conductivity of new polymer electrolytes based on high molecular weight polyether comb polymers. *Electrochim. Acta* **1998**, *43*, 1177–1184. [CrossRef]
73. Scrosati, B. *Advances in Lithium–Ion Batteries*; van Schalkwijk Walter, A., Scrosati, B., Eds.; Kluwer Academic/Plenum Publishers: Norwell, MA, USA, 2002; pp. 252–266.
74. Svanberg, C.; Adebahr, J.; Bergman, R.; Börjesson, L.; Scrosati, B.; Jacobsson, P. Polymer concentration dependence of the dynamics in gel electrolytes. *Solid State Ion.* **2000**, *136–137*, 1147–1152. [CrossRef]
75. Jak, M.J.G.; Ooms, F.G.B.; Kelder, E.M.; Legerstee, W.J.; Schoonman, J.; Weisenburger, A. Design of Organoboron Solid Electrolytes/Solid Electrolyte Interface for Enhanced Performance of Lithium Ion Secondary Batteries. *Power Sources* **1999**, *80*, 83–89. [CrossRef]
76. Tarascon, J.-M.; Gozdz, A.S.; Schmutz, C.; Shokoohi, F.; Warren, P.C. Performance of Bellcore's plastic rechargeable Li-ion batteries. *Solid State Ion.* **1996**, *86–88*, 49–54. [CrossRef]
77. Xu, K. Nonaqueous liquid electrolytes for lithium-based rechargeable batteries. *Chem. Rev.* **2004**, *104*, 4303–4417. [CrossRef] [PubMed]

78. Ue, M.; Mori, S. Mobility and ionic association of lithium salts in a propylene carbonate-ethyl methyl carbonate mixed solvent. *Electrochem. Soc.* **1995**, *142*, 2577–2581. [CrossRef]
79. Schmidta, M.; Heidera, U.; Kuehnera, A.; Oestena, R.; Jungnitza, M.; Ignat'evb, N.; Sartorib, P. Lithium fluoroalkylphosphates: A new class of conducting salts for electrolytes for high energy lithium-ion batteries. *Power Sources* **2001**, *97/98*, 557–560.
80. Walker, C.W., Jr.; Cox, J.D.; Salomon, M. Conductivity and electrochemical stability of electrolytes containing organic solvent mixtures with lithium *tris*(trifluoromethanesulfonyl) methide. *Electrochem. Soc.* **1996**, *143*, L80–L82. [CrossRef]
81. Bates, J.; Dudney, N.; Neudecker, B.; Ueda, A.; Evans, C. Thin-film lithium and lithiumion batteries. *Solid State Ion.* **2000**, *135*, 33–45.
82. Hong, H. Crystal-structure and ionic-conductivity of $li_{14}zn(geo_4)_4$ and other new Li^+ superionic conductors. *Mater. Res. Bull.* **1978**, *13*, 117–124.
83. Seino, Y.; Takada, K.; Kim, B.; Zhang, L.; Ohta, N.; Wada, H.; Osada, M.; Sasaki, T. Synthesis of phosphorous sulfide solid electrolyte and all-solid-state lithium batteries with graphite electrode. *Solid State Ion.* **2005**, *176*, 2389–2393. [CrossRef]
84. Adachi, G.; Imanaka, N.; Aono, H. Fast Li-circle plus conducting ceramic electrolytes. *Adv. Mater.* **1996**, *8*, 127. [CrossRef]
85. Hayashi, A.; Hama, S.; Mizuno, F.; Tadanaga, K.; Minami, T.; Tatsumisago, M. Characterization of Li_2S-P_2S_5 glass-ceramics as a solid electrolyte for lithium secondary batteries. *Solid State Ion.* **2004**, *175*, 683. [CrossRef]
86. Hayashi, A.; Hama, S.; Minami, T.; Tatsumisago, M. Formation of superionic crystals from mechanically milled Li_2S-P_2S_5 glasses. *Electrochem. Commun.* **2003**, *5*, 111. [CrossRef]
87. Machida, N.; Yamamoto, H.; Asano, S.; Shigematsu, T. Preparation of amorphous 75L(2)S center dot chi P2S3 center dot(25-chi)P2S5 (mol%) solid electrolytes by a highenergy ball-milling process and their application for an all-solid-state lithium battery. *Solid State Ion.* **2005**, *176*, 473. [CrossRef]
88. Yamamoto, H.; Machida, N.; Shigematsu, T. A mixed-former effect on lithium-ion conductivities of the Li_2S-GeS_2-P_2S_5 amorphous materials prepared by a high-energy ball-milling process. *Solid State Ion.* **2004**, *175*, 707. [CrossRef]
89. Tatsumisago, M. Glassy materials based on Li_2S for all-solid-state lithium secondary batteries. *Solid State Ion.* **2004**, *175*, 13. [CrossRef]
90. Tatsumisago, M.; Mizuno, F.; Hayashi, A. All-solid-state lithium secondary batteries using sulfide-based glass-ceramic electrolytes. *J. Power Sources* **2006**, *159*, 193. [CrossRef]
91. Koch, C.C. Amorphization by mechanical alloying. *J. Non Cryst. Solids* **1990**, *117*, 670. [CrossRef]
92. Zhou, E.H.; Suryanarayana, C.; Fores, F.H. Effect of premilling elemental powders on solid solubility extension of magnesium in titanium by mechanical alloying. *Mater. Lett.* **1995**, *23*, 27. [CrossRef]
93. Lecaer, G.; Matteazzi, P. Mechanosynthesis of nanocrystalline materials. *Hyperfine Interact.* **1994**, *90*, 229. [CrossRef]
94. Schaffer, G.B.; McCormick, P.G. Reduction of metal-oxides by mechanical alloying. *Appl. Phys. Lett.* **1989**, *55*, 45. [CrossRef]
95. Yu, J.; Chen, Y.; Wuhrer, R.; Liu, Z.W.; Ringer, S.P. In situ formation of BN nanotubes during nitriding reactions. *Chem. Mater.* **2005**, *17*, 5172. [CrossRef]
96. Chen, Y.; Li, C.P.; Chen, H.; Chen, Y.J. One-dimensional nanomaterials synthesized using high-energy ball milling and annealing process. *Sci. Technol. Adv. Mater.* **2006**, *7*, 839. [CrossRef]
97. Wang, J.; Yang, J.; Wan, C.; Du, K.; Xie, J.; Xu, N. Sulfur composite cathode materials for rechargeable lithium batteries. *Adv. Funct. Mater.* **2003**, *13*, 487–492. [CrossRef]
98. Armand, M.; Tarascon, J. Building better batteries. *Nature* **2008**, *451*, 652–657. [CrossRef] [PubMed]
99. Guo, Y.; Hu, J.; Wan, L. Nanostructured Materials for Electrochemical Energy Conversion and Storage Devices. *Adv. Mater.* **2008**, *22*, 4384.
100. Sakuda, A.; Hayashi, A.; Ohtomo, T.; Hama, S.; Tatsumisago, M. All-Solid-State Lithium Secondary Batteries Using $LiCoO_2$ Particles with PLD Coatings of Li_2S-P_2S_5. In *ECS Meeting Abstracts*; IOP Publishing: Bristol, UK, 2010; p. 570.
101. Sata, N.; Eberman, K.; Eberl, K.; Maier, J. Mesoscopic fast ion conduction in nanometre-scale planar heterostructures. *Nature* **2000**, *408*, 946–949. [CrossRef]
102. Trevey, J.E.; Jung, Y.S.; Lee, S.H. Preparation of Li_2S-$GeSe_2$-P_2S_5 electrolytes by a single step ball milling for all-solid-state lithium secondary batteries. *J. Power Sources* **2010**, *195*, 4984–4989. [CrossRef]
103. Trevey, J.; Jang, J.; Jung, Y.; Stoldt, C.; Lee, S. Glass-ceramic Li_2S-P_2S_5 electrolytes prepared by a single step ball billing process and their application for all-solid-state lithium-ion batteries. *Electrochem. Commun.* **2009**, *11*, 1830–1833. [CrossRef]
104. Hayashi, A.; Hama, S.; Morimoto, H.; Tatsumisago, M.; Minami, T. Preparation of Li_2S-P_2S_5 amorphous solid electrolytes by mechanical milling. *J. Am. Ceram. Soc.* **2001**, *84*, 477–479. [CrossRef]
105. Kim, Y.; Martin, S. Ionic conductivities of various GeS_2-based oxy-sulfide amorphous materials prepared by melt-quenching and mechanical milling methods. *Solid State Ion.* **2006**, *177*, 2881–2887. [CrossRef]